Chemistry–A European Journal

Research Article
doi.org/10.1002/chem.202302073

Chemistry Europe
European Chemical Societies Publishing

www.chemeurj.org

Hot Paper

Special Collection

Rational Design, Multistep Synthesis and *in Vitro* Evaluation of Poly(glycerol) Functionalized Nanodiamond Conjugated with Boron-10 Cluster and Active Targeting Moiety for Boron Neutron Capture Therapy

Masahiro Nishikawa,*[a, b] Jie Yu,[a] Heon Gyu Kang,[a] Minoru Suzuki,[c] and Naoki Komatsu*[a]

Dedicated to Professor Maurizio Prato on the occasion of his retirement.

Boron neutron capture therapy (BNCT), advanced cancer treatment utilizing nuclear fission of ^{10}B atom in cancer cells, is attracting increasing attention. As ^{10}B delivery agent, sodium borocaptate (^{10}BSH, $^{10}B_{12}H_{11}SH\cdot 2Na$), has been used in clinical studies along with L-boronophenylalanine. Recently, this boron cluster has been conjugated with lipids, polymers or nanoparticles to increase selectivity to and retentivity in tumor. In this work, anticancer nanoformulations for BNCT are designed, consisting of poly(glycerol) functionalized detonation nanodiamonds (DND–PG) as a hydrophilic nanocarrier, the boron cluster moiety ($^{10}B_{12}H_{11}^{2-}$) as a dense boron-10 source, and phenylboronic acid or RGD peptide as an active targeting moiety. Some hydroxy groups in PG were oxidized to carboxy groups (DND–PG–COOH) to conjugate the active targeting moiety. Some hydroxy groups in DND–PG–COOH were then transformed to azide to conjugate $^{10}B_{12}H_{11}^{2-}$ through click chemistry. The nanodrugs were evaluated *in vitro* using B16 murine melanoma cells in terms of cell viability, BNCT efficacy and cellular uptake. As a result, the $^{10}B_{12}H_{11}^{2-}$ moiety is found to facilitate cellular uptake probably due to its negative charge. Upon thermal neutron irradiation, the nanodrugs with $^{10}B_{12}H_{11}^{2-}$ moiety exhibited good anticancer efficacies with slight differences with and without targeting moiety.

Introduction

Boron neutron capture therapy (BNCT) is an advanced cancer therapy that utilizes nuclear fission reaction of $^{10}B(n,\alpha,\gamma)^{7}Li$.[1–3] Owing to the large neutron absorption cross section of ^{10}B and the short range (<10 μm) of α particle (^{4}He) and lithium nucleus (^{7}Li), cancer cells can be selectively killed by thermal neutron irradiation on a ^{10}B-containing drug delivered in cancer cells. BNCT is attracting much more attentions in recent years since the accelerator-based cancer treatment has obtained regulatory approval in Japan.[4–6] In parallel, a lot of works for BNCT drugs with small compounds, macromolecules or nanomaterials have been reported,[7–23] including poly(glycerol) (PG) functionalized detonation nanodiamonds (DNDs), namely DND–PG, conjugated with ^{10}B-containing moiety we reported recently.[23]

Nanodiamonds (NDs) including DNDs are biologically inert nanoparticles and subjected to various chemical modifications covalently through oxygen containing functional groups on the surface via robust processes.[24–26] In addition, NDs and DNDs possessing fluorescent color centers such as nitrogen vacancy (NV) and silicon vacancy (SiV) centers are expected to be applied to biosensing, imaging and theranostic purposes with non-photo-bleaching or -blinking fluorescence.[27–30] On the other hand, PG functionalization is applied to various nanomaterials in biomedical field due to the hydrophilicity to give them good aqueous dispersibility, high repellent effect against protein adsorption, and abundant hydroxy groups as scaffolds for further chemical functionalization.[23,31–45] Based on these characteristics, DND–PG was conjugated with ^{10}B-enriched phenylboronic acid (PBA) moiety, which played dual roles as a ^{10}B source and a cancer targeting moiety.[19,46,47] Although the resulting DND–PG–PBA suppressed tumor growth *in vivo* upon neutron irradiation, the efficacy was not enough to treat cancer probably due to insufficient ^{10}B content in tumor.

To improve the BNCT efficacy, we designed new DND–PG based nanodrugs conjugated with ^{10}B-enriched sodium boro-

[a] M. Nishikawa, J. Yu, H. G. Kang, Prof. N. Komatsu
Graduate School of Human and Environmental Studies
Kyoto University
Sakyo-ku, 606-8501 Kyoto, (Japan)
E-mail: ma_nishikawa@jp.daicel.com
komatsu.naoki.7w@kyoto-u.ac.jp

[b] M. Nishikawa
Innovation and Business Development Headquarters
Daicel Corporation
1239, Shinzaike, Aboshi-ku, 671-1283 Himeji, Hyogo, (Japan)

[c] Prof. M. Suzuki
Institute for Integrated Radiation and Nuclear Science
Kyoto University
2-1010, Asashiro-nishi, Kumatori-cho, 590-0494 Sennan-gun, Osaka (Japan)

Supporting information for this article is available on the WWW under https://doi.org/10.1002/chem.202302073

This article is part of a joint Special Collection in honor of Maurizio Prato.

captate, or mercaptoundecahydro-*closo*-dodecaborate (^{10}BSH, $^{10}B_{12}H_{11}SH\cdot 2Na$) as a boron-10 source and PBA or RGD peptide as a cancer targeting moiety. ^{10}BSH, which has been used in BNCT clinical studies,[48,49] should increase the boron-10 density due to its icosahedral boron cluster ($^{10}B_{12}H_{11}^{2-}$) containing 12 boron-10 atoms. Whereas the DND–PG moiety is expected to exhibit passive targeting known as EPR effect, we try to increase the targeting efficiency to connect an active targeting moiety; PBA and RGD peptide are known to recognize sialic acid containing sugar chains and $\alpha_v\beta_3$ integrin, respectively, in the tumor cell membrane to facilitate cellular uptake. To introduce these functionalities, some of the primary alcohols in DND–PG were oxidized to carboxy groups according to our recent report to give DND–PG–COOH,[50] where $^{10}B_{12}H_{11}^{2-}$ and PBA or RGD moieties were incorporated at the hydroxy and carboxy groups, respectively. The *in vitro* thermal neutron irradiation resulted in high BNCT efficacies with small differences with and without active targeting moiety. We will discuss these results based on the TEM observation.

Results and Discussion

Synthesis and characterization of BNCT nanodrugs from DND–PG

DND–PG was prepared from aqueous dispersion of single-digit nanometer-sized DND with positive ζ(zeta)-potential (DND(+)) in glycidol as previously reported,[32] and was fully characterized by FT-IR, ^{1}H NMR, elemental analysis and thermogravimetric analysis (TGA) (Supporting Information S1). As shown in Scheme 1a, DND–PG (PG/DND weight ratio: 3.83) was oxidized with 4-AcNH-TEMPO according to our recent paper to give DND–PG–COOH having 1.01 mmol/g of –COOH (see Supporting Information S1 for the experimental detail and Table S1 for characterization data).[50] Some of the OH groups were tosylated under Schotten-Baumann conditions; aqueous dispersion of DND–PG–COOH with NaOH was added to tetrahydrofuran (THF) solution of *p*-toluenesulfonyl chloride (TsCl) with vigorous stirring. Typical reaction conditions, TsCl in pyridine, were not applied, because the raw material was hardly dispersed in

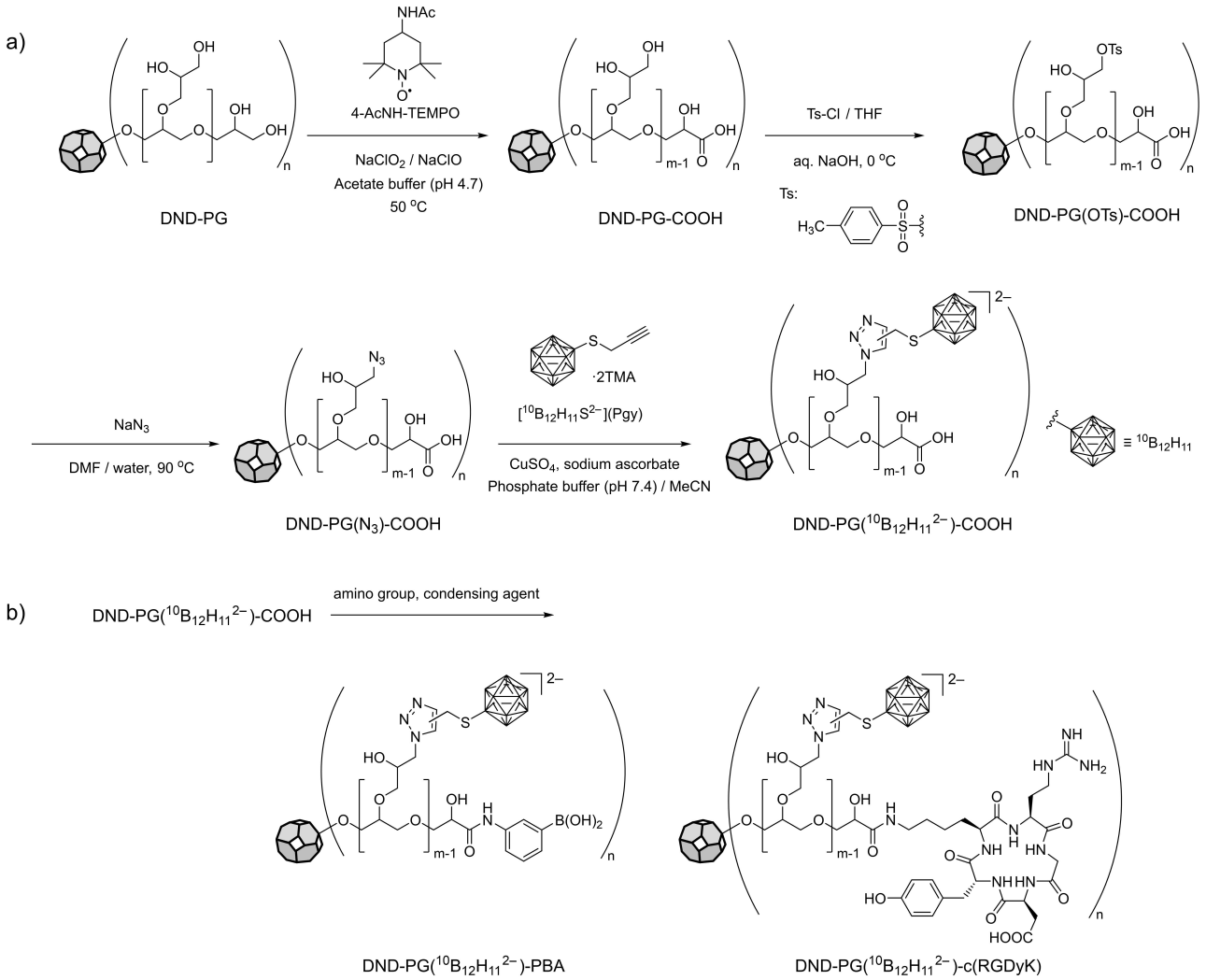

Scheme 1. Synthetic routes of BNCT nanodrugs starting from DND–PG. Introduction of a) $^{10}B_{12}H_{11}^{2-}$ moiety via Hüisgen alkyne-azide cycloaddition (click reaction) at OH group and b) active targeting moieties through amide linkage at COOH group.

pyridine. The loading amount of –OTs was controlled by tuning the amount of TsCl; 1.22 and 0.96 mmol/g of –OTs were obtained by using 7.5 and 5.0 mmol/g of TsCl to the raw material, respectively, which were calculated based on the elemental analysis results (Table S2, and calculation details in Supporting Information S2-1(ii)). On the other hand, 35.4% of PG chain was found to be lost. Although the tosylation was conducted in ice bath, Schotten-Baumann conditions may cleave the ether linkage via β-elimination of –OTs as illustrated in Figure S1.[51] The PG loss of 25% was also observed in the tosylation for DND–PG without carboxylic groups (Table S3), supporting the reaction mechanism through β-elimination under highly basic conditions (Figure S1). The COOH content was accordingly decreased from 1.01 mmol/g to 0.907 mmol/g on DND–PG–COOH, assuming that the proportion of glyceric acid unit was not changed.

The tosyl groups (–OTs) in DND–PG(OTs)–COOH were substituted with azide groups ($-N_3$) by sodium azide (NaN_3) in *N,N*-dimethylformamide (DMF) with small amount of water to obtain DND–PG(N_3)–COOH. Completion of the substitution reaction was confirmed by appearance of the peak for $-N_3$ at 2102 cm^{-1} and disappearance of –OTs at 1176 and 1359 cm^{-1} in FT-IR (Figure 1a and b). The $-N_3$ content in the product, DND–PG(N_3)–COOH, is calculated to be 1.12 mmol/g, indicating that 72.5% of –OTs in DND–PG(OTs)–COOH was converted into $-N_3$ (Table S4 and Supporting Information S2-2).

The $^{10}B_{12}H_{11}^{2-}$ moiety was introduced via μ-alkyne-azide cycloaddition (click reaction).[12–15,45,52,53] *S*-Propargylated boron cluster, [($^{10}B_{12}H_{11}^{2-}$)S](Pgy) was prepared from commercially available ^{10}BSH·2Na via *S*-(2-cyanoethyl) and *S,S*-(2-cyanoethyl)-(2-propynyl)sulfonio derivatives as previously reported (Scheme S1 and experimental details in Supporting Information S3).[13–15] Click reaction between DND–PG(N_3)–COOH and [($^{10}B_{12}H_{11}^{2-}$)S](Pgy) was conducted in the presence of $CuSO_4$ and sodium ascorbate in the mixture of phosphate buffer and acetonitrile (MeCN) in an inert atmosphere. The reaction was monitored by the characteristic peak at 2499 cm^{-1} for B–H stretching vibration of boron cluster in FT-IR as shown in Figure 1c. Small amount of $-N_3$ remained, even though the reaction time was prolonged, probably due to the steric hindrance of icosahedral boron cluster. The resulting DND–PG-($^{10}B_{12}H_{11}^{2-}$)–COOH was characterized by ^{1}H, ^{13}C and ^{10}B NMR. In ^{1}H NMR (Figure 2a), a broad signal around 1.5 ppm and small signals at 8.04 and 8.16 ppm are assigned to hydrogens in boron cluster and 4- or 5-position of 1,2,3-triazole ring, respectively. 1,2,3-Triazole ring is confirmed also by ^{13}C NMR (Figure 2b); the four signals at 125, 137, 143 and 150 ppm are attributable to the carbons in the two isomers of 1,4- and 1,5-disubstituted triazole rings.[54] ^{10}B NMR gives the signal around −16 ppm corresponding to the boron cluster in DND–PG($^{10}B_{12}H_{11}^{2-}$)–COOH (Figure 2c) as well as [($^{10}B_{12}H_{11}^{2-}$)S](Pgy) (Figure S2b).[55] The ^{10}B content in DND–PG-($^{10}B_{12}H_{11}^{2-}$)–COOH was determined to be 7.97% by ICP-AES corresponding to 0.664 mmol/g as $^{10}B_{12}H_{11}^{2-}$ moiety (Table 1)

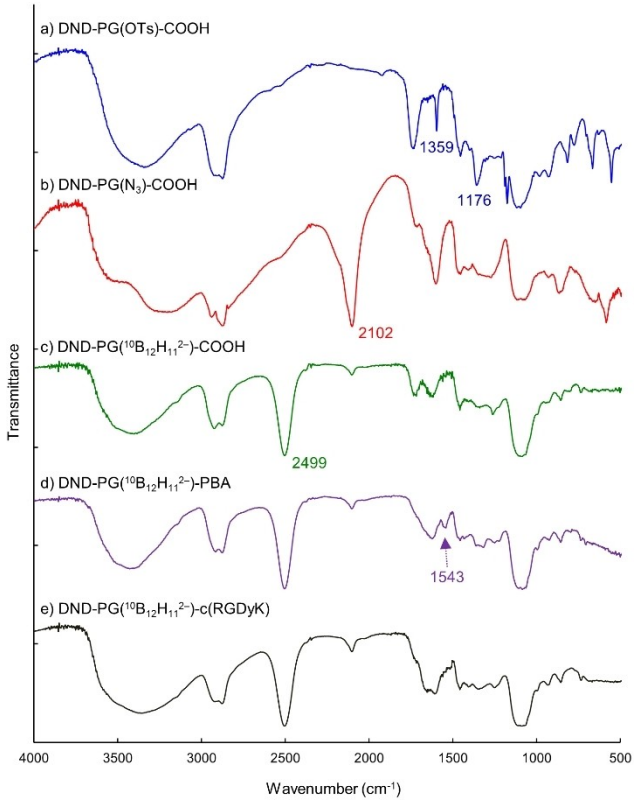

Figure 1. FT-IR spectra of BNCT nanodrugs and intermediates. a) DND–PG-(OTs)–COOH, b) DND–PG(N_3)–COOH, c) DND–PG($^{10}B_{12}H_{11}^{2-}$)–COOH, d) DND–PG($^{10}B_{12}H_{11}^{2-}$)–PBA, and e) DND–PG($^{10}B_{12}H_{11}^{2-}$)–c(RGDyK).

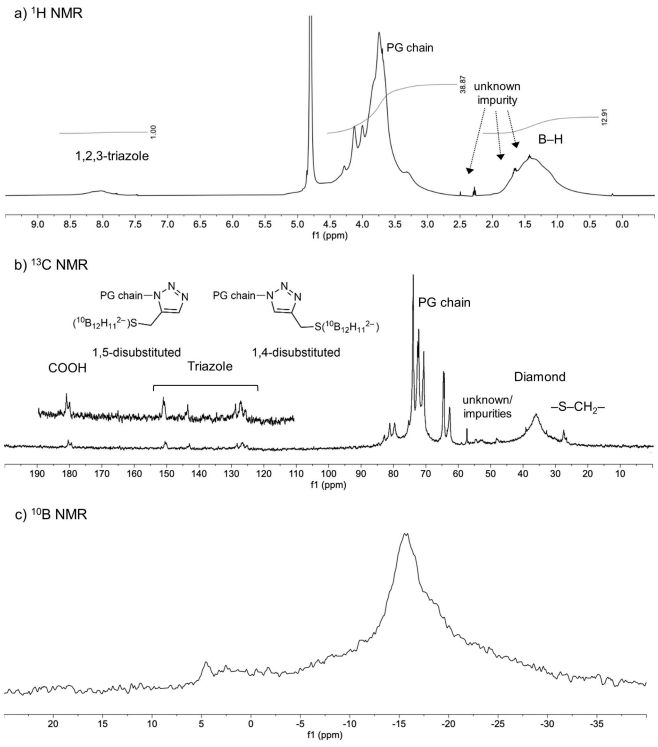

Figure 2. a) ^{1}H NMR, b) ^{13}C NMR by complete decoupling and c) ^{10}B NMR spectra of DND–PG($^{10}B_{12}H_{11}^{2-}$)–COOH in D_2O. The references are set at a) 4.80 ppm (the signal of HOD), b) 36.3 ppm (that of diamond core) and c) 19.49 ppm (that of $^{10}B(OH)_3$ as an external standard).

Table 1. Contents of $^{10}B_{12}H_{11}^{2-}$ and active targeting moieties in nanodrugs.

	$^{10}B_{12}H_{11}^{2-}$ moiety			Active targeting moiety	
	Content (mmol/g)	^{10}B content (%)	Numbers in one particle [a]	Content (mmol/g)	Numbers in one particle [a]
DND-PG($^{10}B_{12}H_{11}^{2-}$)-COOH	0.664	7.97	411	0.74 [b]	455
DND-PG($^{10}B_{12}H_{11}^{2-}$)-PBA	0.633	7.59	391	0.40	259
DND-PG($^{10}B_{12}H_{11}^{2-}$)-c(RGDyK)	0.664	7.97	410	0.0136	8.36

[a] Assuming that PG/DND ratio is 2.49 (see Supporting Information S2-1(ii)) and the diameter of DND core is 5.12 nm.
[b] Content of COOH group.

which is consistent with the estimation from elemental analysis as shown in Table S5 and Supporting Information S2-3. This indicates that 70.8% of $-N_3$ in DND–PG(N_3)–COOH underwent the cycloaddition reaction to bind $^{10}B_{12}H_{11}^{2-}$ moiety covalently.

As active targeting moieties, we chose two kinds of molecules, PBA and RGD peptide (Scheme 1b). PBA is reported to interact with *N*-acetylneuraminic acid (sialic acid) containing sugar chains overexpressed on the surface of cancer cells.[19,46] On the other hand, RGD peptide having Arg-Gly-Asp sequence is known to be an antagonist to integrin $\alpha_v\beta_3$ on cancer cells.[56–58] DND–PG($^{10}B_{12}H_{11}^{2-}$)–COOH was conjugated with 3-aminophenylboronic acid of natural abundance boron through an amide linkage using a condensing agent 1-(3-dimethylaminopropyl)-3-ethylcarbodiimide hydrochloride (EDC) to give DND–PG($^{10}B_{12}H_{11}^{2-}$)–PBA. The DND–PG($^{10}B_{12}H_{11}^{2-}$)–COOH with the COOH content of 0.74 mmol/g was reacted with about 0.56 mmol/g (0.76 eq. to –COOH) of 3-aminophenylboronic acid. This resulted in the PBA of 0.40 mmol/g in DND–PG-($^{10}B_{12}H_{11}^{2-}$)–PBA, or 0.42 mmol/g of DND–PG($^{10}B_{12}H_{11}^{2-}$)–COOH (Table 1, Table S6 and Supporting Information S2-4), which corresponds to 75% yield based on 3-aminophenylboronic acid. The ^{10}B content was estimated to be 7.59%. For characterization of DND–PG($^{10}B_{12}H_{11}^{2-}$)–PBA, broad signals between 7–8 ppm are assigned to aromatic protons in PBA moiety in ^{1}H NMR (Figure S3a), and the amide linkage was confirmed by stretching vibration of carbonyl group at 1543 cm^{-1} in FT-IR (Figure 1d).

The RGD peptide was conjugated with DND–PG($^{10}B_{12}H_{11}^{2-}$)–COOH through amide linkage at ε-amino group in a cyclic pentapeptide, cyclo(L-Arg-Gly-L-Asp-D-Tyr-L-Lys) (c(RGDyK)), with EDC and *N*-hydroxysuccinimide (HOSu). Introduction of c(RGDyK) was confirmed by ^{1}H NMR with a pair of small signals of aromatic ring in Tyr at 6.56 and 6.95 ppm (Figure S3b). From the integration value, the loading amount is estimated to be 0.014 mmol/g (Table S7 and Supporting Information S2-5) that is very small as compared with the amount of c(RGDyK)·2TFA (0.46 mmol/g, or 0.62 eq. to –COOH) used for the reaction. As summarized in Table 1, assuming the diameter of DND core to be 5.12 nm, it can be calculated that 8.4 molecules of c(RGDyK) in average are attached in a particle of DND–PG($^{10}B_{12}H_{11}^{2-}$)–c-(RGDyK) while ca. 5×10^3 of glycerol and glyceric acid units are contained.[32] The nanomaterials (nanodrugs) without $^{10}B_{12}H_{11}^{2-}$ moiety, DND–PG–PBA and DND–PG–c(RGDyK), were also prepared by the same procedures shown in Scheme 1b from DND–PG–COOH (data not shown).

In vitro evaluation of BNCT nanodrugs by cell viability assay

Cell viability assay was conducted with the following nanodrugs; DND–PG–COOH, –PBA and –c(RGDyK) with and without $^{10}B_{12}H_{11}^{2-}$ moiety as shown in Figure 3. In this work, we chose B16 murine melanoma cells, because they are reported to interact with PBA and RGD peptide,[19,58] and melanoma is one kind of tumors to which BNCT has been applied in clinical trials.[59]

The cells were incubated in nanodrug-containing culture medium supplemented with and without fetal bovine serum (FBS) for 1 d (FBS(+) and FBS(−), respectively). The nanodrug concentrations were 125, 250 and 500 μg/mL for FBS(+), and 63, 125 and 250 μg/mL for FBS(−). Sample concentrations in FBS(−) was lowered by half of that in FBS(+) since the toxicity in FBS(−) was estimated to be higher than that in FBS(+).[35]

In the presence of FBS (Figure 3a), the nanodrugs with $^{10}B_{12}H_{11}^{2-}$ moiety exhibited toxicity depending on the concentration (500 > 250 > 125 μg/mL) and functionality (c(RGDyK) > PBA ≈ COOH), while the samples without $^{10}B_{12}H_{11}^{2-}$ moiety showed little or no toxicity. The nanodrugs are more toxic under FBS(−) conditions than FBS(+) ones as shown in Figure 3b and Figure S4; in particular, the difference is more significant in the cases of DND–PG–c(RGDyK), DND–PG-($^{10}B_{12}H_{11}^{2-}$)–PBA and DND–PG($^{10}B_{12}H_{11}^{2-}$)–c(RGDyK). These results will be discussed below based on TEM analysis (Figure 5).

In vitro evaluation of BNCT nanodrugs by colony forming assay

BNCT efficacies of nanodrugs were examined on thermal neutron irradiation. After the treatment with nanodrug, detached cells were irradiated with thermal neutron. On the neutron irradiation at 1.19×10^{12}–3.47×10^{12} neutrons/cm^2, no or only a few colonies were found at 500 μg/mL for DND–PG-($^{10}B_{12}H_{11}^{2-}$)–COOH and –PBA, and 125 μg/mL for DND–PG-($^{10}B_{12}H_{11}^{2-}$)–c(RGDyK) under FBS(+) conditions (Figure S5 and Table S8), corresponding to 39.9, 38.0 and 9.9 μg/mL in ^{10}B

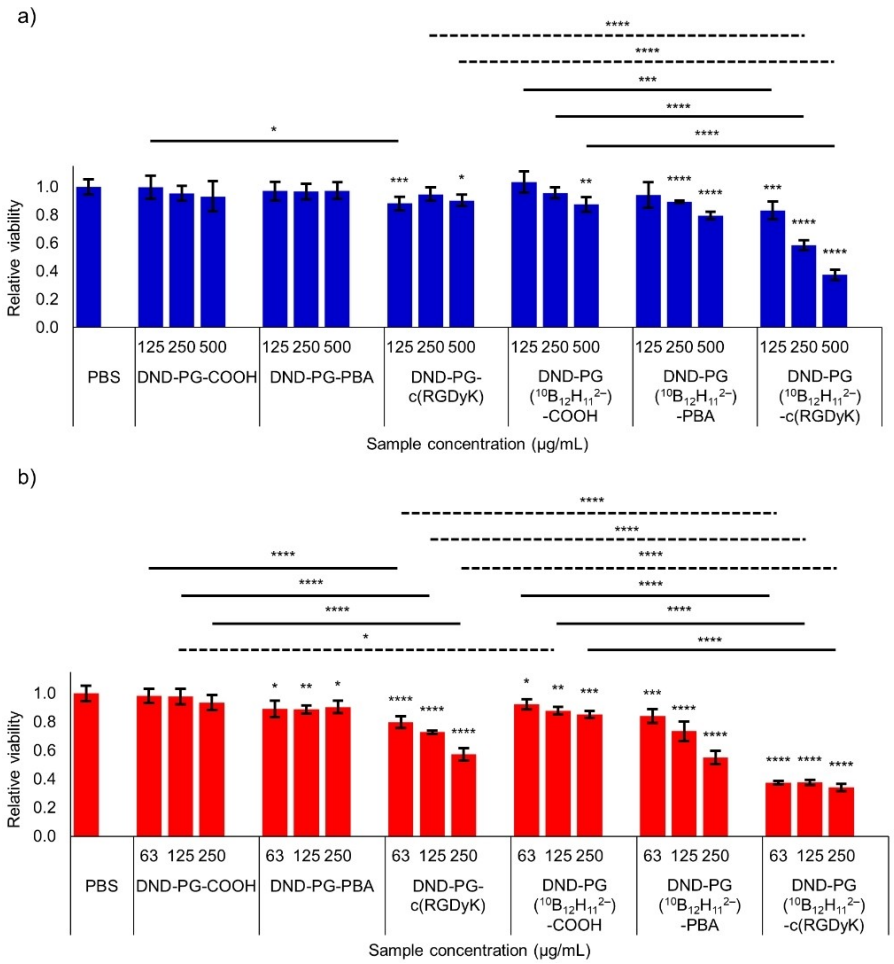

Figure 3. Cell viability of B16 murine melanoma cells with and without FBS (FBS(+) in a) and FBS(−) in b), respectively) at various nanodrug concentrations. Asterisks on each bar indicate the significancy to control (PBS). Lines with asterisks on each panel indicate the significancy between with and without c(RGDyK) moiety (solid lines) or $^{10}B_{12}H_{11}^{2-}$ moiety (dashed lines) ($n = 6$, Student's t-test in comparison with PBS, and 2-way ANOVA and Tukey's HSD test for comparison between nanodrugs: * $p < 0.05$, ** $p < 0.01$, *** $p < 0.001$, *** $p < 0.0001$). See Figure S4 to compare the results at the same concentration levels (125 and 250 μg/mL).

concentrations, respectively, while the nanomaterials without $^{10}B_{12}H_{11}^{2-}$ moiety exhibited no BNCT efficacy. Therefore, the corresponding concentrations and fluences were reduced to 200 and 100 μg/mL (ca. 16 and 8 μg/mL of ^{10}B, respectively) and 4.09×10^{11}–1.17×10^{12} neutrons/cm^2.

High BNCT efficacies along with the concentration and fluence relationship were observed as shown in Figure 4 and Table S9. Similar BNCT efficacies were observed in the three nanodrugs with $^{10}B_{12}H_{11}^{2-}$ moiety. The significant difference ($p = 0.014$) is found only in the slopes between DND–PG-($^{10}B_{12}H_{11}^{2-}$)–PBA and –c(RGDyK) at 200 μg/mL (blue and green dashed lines, respectively, in Figure 4). The comparison between FBS(+) and (−) conditions in thermal neutron irradiation was additionally conducted at the ^{10}B concentration of ca. 12 μg/mL (200 μg/mL of nanodrug containing 5.8–6.1 % of ^{10}B). As shown in Figure S6 and Table S10, FBS(−) exhibited higher BNCT efficacy than FBS(+) in all three nanodrugs, DND–PG($^{10}B_{12}H_{11}^{2-}$)–COOH, –PBA and –c(RGDyK). Although DND–PG($^{10}B_{12}H_{11}^{2-}$)–c(RGDyK) and –COOH gave no colonies under FBS(−) conditions, DND–PG($^{10}B_{12}H_{11}^{2-}$)–PBA exhibited the significant difference in the slopes under FBS(+) and (−) conditions. These results will be interpreted by TEM observation in the next section.

TEM analysis of cells after Incubation with nanodrugs

To interpret the cytotoxicity and BNCT efficacy mentioned above, the cells treated with nanodrug under FBS(+) and FBS(−) conditions were analyzed by TEM. Concentrations of the nanodrugs were 100 and 750 μg/mL for the ones with and without $^{10}B_{12}H_{11}^{2-}$ moiety, respectively. Because no nanoparticles were observed in the TEM images of the nanodrugs without $^{10}B_{12}H_{11}^{2-}$ moiety at 200 μg/mL in our preliminary experiment (data not shown), much higher concentration (750 μg/mL) was applied. In addition, the nanodrugs should be taken up by the cells not through precipitation, but from the medium, because hydrodynamic diameters of the nanodrugs with and without FBS clearly indicate no significant aggregation

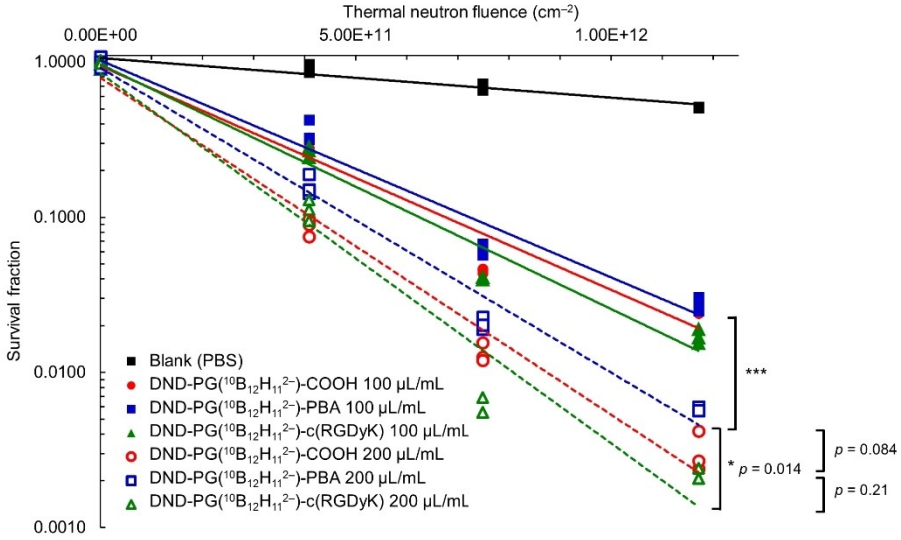

Figure 4. Result of colony forming assay on B16 cells exposed to $^{10}B_{12}H_{11}^{2-}$ functionalized nanodrugs and irradiated by thermal neutron. Solid lines are the fitted curves in exponential approximation for nanodrugs in the same colors at 100 μg/mL. The dashed lines are for nanodrugs at 200 μg/mL. (Significance in the difference of slopes after the logarithmic conversion: $*p < 0.05$, $**p < 0.01$, $***p < 0.001$)

(Figure S7) due to the high hydrophilicity and protein repellent property of PG mentioned above.

The black dots in vesicles in Figure 5, which are made to be clearer in the expanded images (Figure S8a–h) and images of different sights (Figure S8i–k), are assigned to be DND particles of nanodrugs, because they were not observed in control cells (Figure 5a) and loomed out in white (Figure S9) when TEM was defocused. In addition, boron was detected by energy dispersive X-ray spectroscopy with scanning electron microscopy (SEM-EDS) as shown in Figure S10, where a shoulder peak was observed at the energy of B*K* in some vesicles containing black dots (Figure S10b, c and d).

Similar numbers of the black dots in vesicles with 200–400 nm size were observed in the cells treated with DND–PG-($^{10}B_{12}H_{11}^{2-}$)–COOH, –PBA and –c(RGDyK) (100 μg/mL in culture medium) under FBS(+) conditions (Figure 5b, c and d, respectively). The above results of similar BNCT efficacies among the three nanodrugs can be interpreted by these TEM observations. Much less numbers of black dots were found in the cases of DND–PG–PBA and –c(RGDyK) (750 μg/mL in culture medium) under FBS(+) conditions (Figure 5f and g, respectively), while no black dots were observed in the cell treated with DND–PG–COOH at the same concentration (Figure 5e). Although active targeting capability of PBA and c(RGDyK) is observed in the absence of $^{10}B_{12}H_{11}^{2-}$ moiety, it seems to be hidden by $^{10}B_{12}H_{11}^{2-}$ moiety, which is considered to facilitate cellular uptake more than the active targeting moieties of PBA and c(RGDyK). This may be attributed to the dianionic nature of the boron cluster, which can interact electrostatically with the proteins in cell membrane and in serum to induce cellular uptake.[60–62] The higher toxicity of DND–PG($^{10}B_{12}H_{11}^{2-}$)–c(RGDyK) than DND–PG($^{10}B_{12}H_{11}^{2-}$)–COOH and –PBA shown in Figure 3a and b implies that c(RGDyK) is much more toxic than COOH and PBA by taking into consideration the large difference in their numbers in one particle as shown in Table 1.

On the other hand, the sizes of vesicles containing DND–PG($^{10}B_{12}H_{11}^{2-}$)–COOH, –PBA and –c(RGDyK) under FBS(–) conditions are larger than those under FBS(+) conditions as shown in Figure S9. This indicates that the numbers of nanoparticles taken up by the cells are larger under FBS(–) conditions than FBS(+) ones, leading to the higher BNCT efficacies as described above (Figure S6 and Table S10). This implies that the electrostatic interaction of $^{10}B_{12}H_{11}^{2-}$ moiety with the membrane proteins induces the cellular uptake more efficiently under FBS(–) conditions than FBS(+) ones, where the serum proteins adsorbed electrostatically by $^{10}B_{12}H_{11}^{2-}$ (Figure S13 and Supporting Information S9) would reduce the cellular uptake efficiency.[33–35,61]

Conclusions

We designed boron delivery agent for BNCT based on PG functionalized DND with a boron cluster and an active targeting moiety. To construct the nanodrug, $^{10}B_{12}H_{11}^{2-}$ moiety was first conjugated by click chemistry at the –OH groups of ND–PG–COOH, which is prepared by oxidation of DND–PG. Then, PBA or c(RGDyK) moiety for active targeting was introduced at the –COOH groups through amide linkage. The nanodrugs have ^{10}B content of 7.6–8.0% that is much higher than that of our previous BNCT nanodrug and exhibit good dispersibility under physiological conditions.[23]

In vitro neutron irradiation experiments exhibited high BNCT efficacies in nanodrugs with $^{10}B_{12}H_{11}^{2-}$ moiety, showing small differences with and without targeting moieties. TEM observations of the cells treated with the nanodrugs indicate that $^{10}B_{12}H_{11}^{2-}$ moiety itself facilitates cellular uptake much

more than the active targeting moieties of PBA and c(RGDyK), resulting in similar BNCT efficacies among these nanodrugs.

The nanodrug with $^{10}B_{12}H_{11}^{2-}$ moiety based on DND–PG–COOH would serve as a lead material of boron delivery agent for BNCT. However, we have to consider the improvement of active targeting efficiency. The multiple functionalization process we designed and achieved in this work is so flexible that it can be applied to nanodrugs with a variety of structural and functional features. Therefore, we are expecting to create more effective nanodrugs for BNCT in near future.

Experimental Section

Materials

Single-digit nanometer-sized water dispersion of DNDs was manufactured by Daicel Corporation (DINNOVARE™). For the modification of DNDs, the following reagents and solvents were purchased from FUJIFILM Wako Pure Chemical Corporation (Osaka Japan); sodium hypochlorite (NaClO) solution, sodium azide (NaN_3), acrylonitrile, ethylenediamine-*N,N,N′,N′*-tetraacetic acid disodium salt (EDTA·2Na, produced by Dojindo Laboratories, Japan), hydrochloric acid (HCl), sodium hydroxide (NaOH), ethanolic solution of potassium hydroxide (KOH), acetic acid, sodium acetate, potassium dihydrogen phosphate, ethylene glycol, tetrahydrofuran (THF), *N,N*-dimethylformamide (DMF), acetonitrile (MeCN), ethyl acetate, 0.25% trypsin-EDTA·4Na solution, Dulbecco's phosphate-buffered saline (pH 7.4, PBS(−)), 10x PBS(−), sodium dodecyl sulfate (SDS) and cell counting kit-8 (CCK-8, a formulation of 2-(2-methoxy-

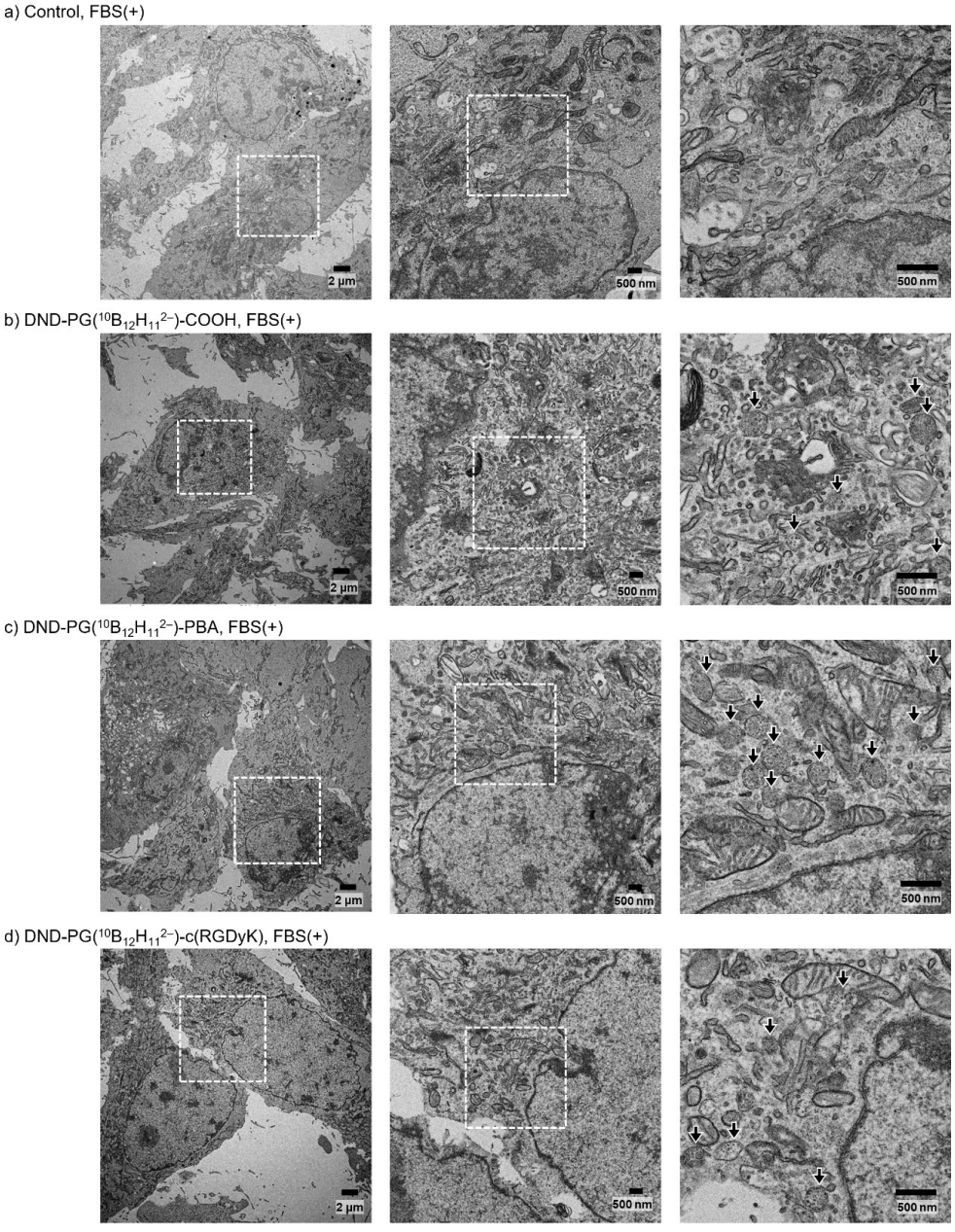

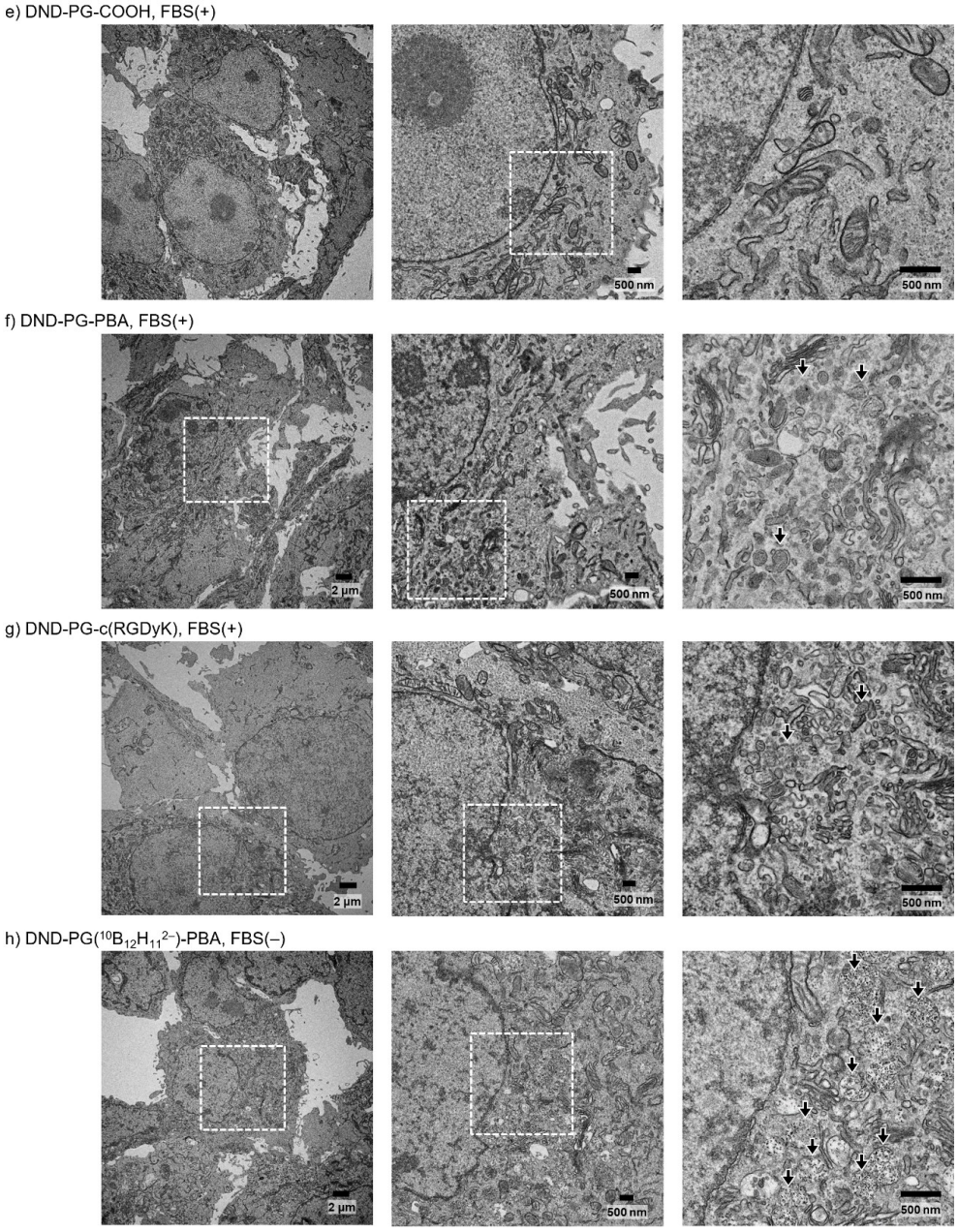

Figure 5. TEM images of B16 cells treated with nanodrugs under FBS(+) or FBS(−) conditions (accelerating voltage: 80 keV). Images of cells with each material consist of three images of different magnifications. Squares with white dashed lines indicate the areas of expansion that are shown on the right. Black arrows indicate the location of vesicles including dots of nanoparticles (all vesicles are not necessarily pointed).

4-nitrophenyl)-3-(4-nitrophenyl)-5-(2,4-disulfophenyl)-2*H*-tetrazolium, monosodium salt (WST-8) and 1-methoxy-5-methylphenazinium methylsulfate (1-methoxy PMS), produced by Dojindo Laboratories, Japan). 4-acetamido-2,2,6,6-tetramethylpiperidine-1-oxyl free radical (4-AcNH-TEMPO), *p*-toluenesulfonyl chloride (Ts–Cl), tetramethylammonium hydroxide (TMAOH) methanol solution (10%), propargyl bromide, sodium ascorbate, 3-aminophenylboronic acid monohydrate (natural abundance boron) and 2-(*N*-morpholino)ethanesulfonic acid (MES) were purchased from Tokyo Chemical Industry Co., Ltd. (Tokyo Japan). Sodium mercaptoundecahydro-*closo*-dodecaborate(^{10}B) (^{10}BSH) was purchased from Katchem spol. s r. o. (Czech). *N*-hydroxysuccinimide (HOSu) from Peptide Institute, Inc. was used. 4% Paraformaldehyde in phosphate buffer produced by Muto Pure Chemicals Co., Ltd was used. Cyclo-(L-Arg-Gly-L-Asp-D-Tyr-L-Lys) trifluoroacetic acid salt (c(RGDyK)·2TFA) was purchased from Hanzhou Taijia Biotech Co., Ltd. Copper sulfate ($CuSO_4$, anhydrous) was purchased from Kishida Chemical Co., Ltd. (Osaka Japan). Sodium chlorite ($NaClO_2$) was purchased from Sigma-Aldrich Japan G. K. (Tokyo, Japan). 1-(3-Dimethylaminopropyl)-3-ethylcarbodiimide hydrochloride (EDC) is a product of Kokusan Chemical Co., Ltd. Antibiotics solution (penicillin-streptomycin-amphotericin B, 100x) was purchased from Thermo Fisher Scientific (MA USA). Dulbecco's modified Eagle Medium (DMEM, Glucose 4.5 g/L), PBS and 0.5% trypsin-EDTA·4Na solution, crystal violet, 25% glutaraldehyde (for electron microscopy), methanol and ethanol from Nacalai Tesque, Inc. (Kyoto Japan) were used. Fetal bovine serum (FBS) was supplied by Biosera Inc.

(France). Bicinchoninic acid (BCA) assay was done with TaKaRa BCA protein assay kit (Takara Bio, Japan).

Equipment

^{1}H, ^{13}C and ^{10}B NMR spectra were measured with an ECX500 NMR spectrometer (JEOL). FT-IR spectra were recorded on an IR Tracer-100 FT-IR spectrometer (Shimadzu) equipped with DiffusIR DRIFT chamber (PIKE Technologies). Elemental analyses were conducted at Organic Elemental Microanalysis Centre of Kyoto University. ICP-AES analysis for boron content was done with an SPS3100 (SII Nanotechnology) at Nippon Steel Technology Co., Ltd. ESI-MS was measured with micrOTOF mass spectrometer (Bruker). TGA was performed with TG/DTA 6200 (SII). ζ-Potential was measured by ZetaSizer Nano (Malvern, UK). DLS measurement was done by Nanotrac Wave II particle size analyzer (MicrotracMRB). The absorbance of CCK-8 and BCA was measured with a microplate reader MTD-310 (Corona Electric Co., Japan). TEM observation of cells was performed on a H-7650 transmission electron microscope (Hitach, Japan). Energy dispersive X-ray spectroscopy (SEM-EDS) was measured with JSM7900F scanning electron microscope (JEOL, Japan).

DND–PG(OTs)–COOH

To the water suspension of DND–PG–COOH (2.95% (w/w), 13.5 g, net 0.40 g, PG/DND 3.85, COOH content 1.01 mmol/g), water 2.45 mL and 8 M NaOH (3.0 mL, 24 mmol) were added, and the mixture was cooled in ice-bath. THF (3.6 mL) solution of Ts–Cl (0.58 g, 3.0 mmol) was added in an intermittent manner for about 1 h with vigorously stirring. The reaction was stirred for more 2 h under ice-cooled condition, then added 6 M HCl (4.0 mL) to acidify and stirred for several hours. The mixture was centrifuged (3000 rpm, 30 min). The precipitate was washed three times by the addition of small amount of THF (2–3 mL) and water (10–15 mL) followed by centrifugation or ultra-centrifugation (183400*g*, 30 min) according to the state of dispersion in supernatant to give the precipitate as much as possible. The precipitate was dispersed in DMF (20 mL) and ultra-centrifuged. This operation was repeated once as solvent substitution, and DMF dispersion (18.5 g) of DND–PG(OTs)–COOH was obtained. The concentration was determined to be 1.48% (w/w) and net yield was 0.27 g. Elemental analysis: C; 56.85%, H: 6.53%, N; 0.51%, O; 29.08%, S; 4.08%.

DND–PG(N_3)–COOH

DMF suspension of DND–PG(OTs)–COOH (1.48% (w/w), 13.8 g, net 0.20 g) was added with NaN_3 (196 mg, 3.0 mmol), water (3.0 mL) and 1 M NaOH (0.30 mL, 0.30 mmol). The mixture was stirred at 60 °C for 0.5 h, then the temperature was raised to 90 °C for 18 h. Resulting cloudy suspension was ultra-centrifuged (183400*g*, 2 h) and the precipitate was washed with water three times by the dilution and ultra-centrifugation. The precipitate was dispersed in water (30.0 g). The concentration was determined to be 0.57% (w/w) and net yield was 0.17 g. Elemental analysis: C; 55.28%, H: 5.54%, N; 5.46%, O; 30.96%.

DND–PG($^{10}B_{12}H_{11}^{2-}$)–COOH

Aqueous dispersion of DND–PG(N_3)–COOH (0.57% (w/w), 8.84 g, net 50.1 mg) was added with MeCN (4.0 mL), 0.4 M phosphate buffer (pH 7.4, 2.5 mL), sodium ascorbate (42.2 mg, 0.21 mmol) and bis-tetramethylammonium *S*-(propyn-3-yl)thioundecahydro-*closo*-dodecaborate(^{10}B) [($^{10}B_{12}H_{11}^{2-}$)S](Pgy)·2TMA, crude, 50.3 mg, starting from 21.1 mg of $^{10}BSH \cdot 2Na$ (0.10 mmol)), and the mixture was vacuum degassed with sonication. Aqueous solution of $CuSO_4$ (14.2 mg, 0.088 mmol in 0.50 mL water) was added slowly, then the reaction was stirred under nitrogen atmosphere at room temperature. The reaction was monitored by FT-IR (absorbances of azide and B–H at 2102 cm^{-1} and 2503 cm^{-1}, respectively) of sample taken from the reaction. As not negligible peak of azide remained, [($^{10}B_{12}H_{11}^{2-}$)S](Pgy)·2TMA (crude, 24.8 mg in total of three-time addition), sodium ascorbate (10.3 mg) and $CuSO_4$ (3.4 mg in small amount of water) were added after 22–30 h from the start. The reaction was stirred for more two days. Resulting dark-brown dispersion was ultra-centrifuged (183400*g*, 30 min) and the precipitate was washed with water (10 mL), aqueous solution of EDTA·2Na (0.3%, 10 mL, two times) and water (10 mL, three times) using centrifuge filter (Amicon® Ultra, 30 kDa). The concentrate on the filter was diluted with water to give dark-brown dispersion (10.1 g). The concentration was determined to be 0.50% (w/w) from the weight after lyophilization, and net yield was 50.5 mg. Elemental analysis: C; 48.22%, H: 5.33%, N; 3.78%. ^{10}B content (ICP-AES by alkaline fusion method for specimen preparation): 7.97%.

DND–PG($^{10}B_{12}H_{11}^{2-}$)–PBA

Aqueous dispersion of DND–PG($^{10}B_{12}H_{11}^{2-}$)–COOH (0.50% (w/w), 5.0 g, net 25.0 mg) was added with aqueous solution of MES (0.1 M, pH was adjusted to 4.5, 2.0 mL), 3-aminophenylboronic acid monohydrate (0.22 mL of 1.0 wt% DMF solution, 2.2 mg, 0.014 mmol) and EDC (0.50 mL of 1.0 wt% aqueous solution, 5.0 mg, 0.026 mmol). The mixture was stirred at room temperature for 15 h. After the reaction, pH was adjusted 10.0 with 1 M NaOH and the mixture was stirred for 45 min. The dispersion was ultra-filtered and then washed with water five times. The concentrate on the filter was diluted with water to give dark-brown dispersion (4.91 g). The concentration was determined to be 0.50% (w/w) from the weight after lyophilization, and net yield was 24.6 mg. Elemental analysis: C; 51.35%, H: 5.10%, N; 4.16%.

DND–PG($^{10}B_{12}H_{11}^{2-}$)–c(RGDyK)

Aqueous dispersion of DND–PG($^{10}B_{12}H_{11}^{2-}$)–COOH (0.50% (w/w), 3.4 g, net 16.9 mg) was added with phosphate buffer (0.4 M, pH 7.4, 2.0 mL), HOSu (0.47 mL of 1.0 wt% water solution, 4.7 mg, 0.041 mmol) and EDC (0.39 mL of 1.0 wt% aqueous solution, 3.9 mg, 0.020 mmol). The mixture was stirred at room temperature for 30 min. Then, c(RGDyK)·2TFA (7.4 mg, 0.0087 mmol) was added and the mixture was stirred at room temperature for 24 h. The dispersion was ultra-filtered and then washed with water six times. The concentrate on the filter was diluted with water to give dark-brown dispersion (1.70 g). The concentration was determined to be 0.85% (w/w) from the weight after lyophilization, and net yield was 14.5 mg.

Cell viability assay with CCK-8

B16 mouse melanoma cells were seeded on 96-well microplates by 3×10^3 cells/well in 100 μL of DMEM (Glucose 4.5 g/L) culture medium (supplemented with 10% FBS and 1% of 100x penicillin-streptomycin-amphotericin B solution) for each well. After incubation in CO_2 incubator at 37 °C for 3 d, culture medium (100 μL) was replaced once, PBS (as control) or PBS dispersion of nanoparticles (2500, 1250 and 625 μg/mL, 25 μL for each) were added, and the cells were further incubated for 24 h. Under FBS(−) conditions, replacement of culture medium was done with DMEM that was not supplemented with FBS, and the concentrations of nanoparticles were 1250, 625 and 312.5 μg/mL in PBS. The cells were washed

with culture medium (two times) and PBS, CCK-8 in culture medium (10 μL of CCK-8 and 100 μL medium for each well) was added. After 0.5 h, the absorbance at 450 nm was measured for each well using the microplate reader.

Colony forming assay on thermal neutron irradiation

B16 cells (8.8×10^5 or 1.0×10^6 cells) in 10 mL DMEM culture medium (glucose 4.5 g/L, with 10% FBS and antibiotics/antimycotic) were seeded on 100 mmφ dishes, and incubated in CO_2 incubator at 37 °C for 2 d. The culture medium (10 mL, with or without FBS for FBS(+) or FBS(−) condition, respectively) was replaced once, PBS or PBS dispersion of nanoparticles (1.0 mL) were added to make predetermined sample concentrations in the medium. After incubated in CO_2 incubator at 37 °C for 22–24 h, the cells were washed with PBS and detached by treatment with trypsin (0.5%, 2.0 mL) at 37 °C for 5 min. After trypsinization was terminated with culture medium (with FBS), the number of cells was counted and adjusted the concentration to 100000 cells/mL, then the suspension of cells was dispensed into four plastic tubes by 1 mL/tube. Thermal neutron irradiation was conducted at KUR nuclear reactor (Kumatori campus, Kyoto University) at three levels of irradiation doses (for example, 5, 10 and 15 min of irradiation time in 1 MW output, corresponding to the fluence of 4.09×10^{11}, 7.48×10^{11} and 1.17×10^{12} neutrons/cm^2, respectively), and one tube for the control without the irradiation. The thermal neutron fluence was determined by averaging gold foils attached to the surface of the tube along the direction of incidence of the thermal neutrons. The cells were seeded on 60 mmφ dishes placed 5 mL culture medium (with FBS) by predetermined numbers (300–10000 cells/dish, see Tables S8–S10). After incubation in CO_2 incubator at 37 °C for 9–11 days, resulting colonies were fixed with 70% ethanol and stained with 0.1% crystal violet solution. The numbers of colonies were counted by visual examination (naked eyes).

Analysis of total adsorbed protein (protein corona) by BCA assay

Mixtures of PBS dispersion (900 μL) of nanodrugs (net 0.20–1.0 mg) and FBS (100 μL) were incubated at 37 °C for 1 h. The mixtures were ultracentrifuged (434000 *g*, 20 min). The lower layers (ca. 100 μL including pellet) were washed with water 3 times by repeating re-dispersion (total volume 1.0 mL) – ultracentrifugation procedures. SDS solution (20%, 100 μL) was added to each lower layer (ca. 100 μL) and ultracentrifuged. Resulting supernatant was transferred to 96-well microplate (20 μL×4 wells for each material), and then PBS (80 μL), the mixture of solutions (100 μL) of reagent A and B of BCA assay kit were added. After the incubation at 37 °C for 1 h, absorbance of 570 nm was measured by the microplate reader. Calibration curve was created using BSA (bovine serum albumin) standard solution. The results are shown in Figure S13.

TEM observation of cellular uptake

B16 cells were seeded on 8-well chamber slide (Nagel Nunc 177445) by 2.5×10^4 cells/well (3.0×10^4 cells/cm^2) in 400 μL of DMEM (Glucose 4.5 g/L, with 10% FBS) culture medium. After incubation in CO_2 incubator at 37 °C for 3 d, culture medium (400 μL, with or without FBS for FBS(+) or FBS(−) condition, respectively) was replaced once, PBS (control) or PBS dispersion of nanoparticles were added at predetermined concentration of each nanodrug, and the cells were further incubated for 24 h. The cells were washed with culture medium (two times) and PBS, then fixed in the mixture of 25% glutaraldehyde and 4% paraformaldehyde in 0.1 M phosphate buffer (1/10 (v/v)) for a couple of days in the refrigerator. Then the fixed cells were incubated with 1.5% potassium ferrocyanide followed by 2% osmium tetroxide in deionized water (DW) at 4 °C. After 1 h, the cells were washed with distilled water (DW) and fixed with 2% osmium tetroxide in DW at room temperature for 1 h. The specimens were then stained en bloc in a solution of 4% uranyl acetate dissolved in DW overnight for contrast enhancement and then washed with DW. Subsequently, the specimens were further stained with Walton's lead aspartate solution for 2 h, dehydrated with a dilution series of ethanol (60%, 70%, 80%, 90%, 99%, and 100%) and embedded in Epon 812. Ultra-thin sections were made using an ultramicrotome (Leica UC7). Sections were stained with uranyl acetate and lead citrate and observed under an H-7650 electron microscope (HITACHI).

Statistical analysis

The differences between the groups were evaluated using Student's t test for two groups and a two-way analysis of variance (ANOVA) followed by Tukey's HSD test for multiple groups. For BNCT efficacy, significancy between the slope of fitted curve was evaluated.

Acknowledgements

We acknowledge Dr. Yoshinori Sakurai and Dr. Takushi Takata (Kyoto University) for experimental help of the neutron irradiation. We also thank T. Katsuno, H. Kohda and K. Okamoto-Furuta (Kyoto University) for their help with sample preparation for TEM and SEM-EDS analyses, and valuable discussion. For the analysis of boron content, we appreciate Y. Yamamoto, C. Tagawa, S. Tada and J. Kuwana (Daicel Corporation).

Conflict of Interests

M. N. and N. K. are inventors on Japanese patent application number 2022-028954 submitted by Kyoto University and Daicel Corporation. It covers PG-functionalised nanoparticles in which at least one –CH_2OH is substituted by –COOH described in this manuscript. Other authors declare no conflicts of interest.

Data Availability Statement

The data that support the findings of this study are available in the supplementary material of this article.

Keywords: boron cluster · boron neutron capture therapy (BNCT) · nanodiamond · poly(glycerol) functionalization

[1] M. Suzuki, *Int. J. Clin. Oncol.* **2020**, *25*, 43–50.
[2] M. A. Dymova, S. Y. Taskaev, V. A. Richter, E. V. Kuligina, *Cancer Commun.* **2020**, *40*, 406–421.
[3] R. F. Barth, J. C. Grecula, *Appl. Radiat. Isot.* **2020**, *160*, 109029.
[4] Y. Kiyanagi, Y. Sakurai, H. Kumada, H. Tanaka, *AIP Conf. Proc.* **2019**, *2160*, 050012.
[5] S. Kawabata, M. Suzuki, K. Hirose, H. Tanaka, T. Kato, H. Goto, Y. Narita, S. Miyatake, *Neuro Oncol. Adv.* **2021**, *3*, 1–9.

[6] D. E. Cartelli, M. E. Capoulat, M. Baldo, J. C. Suarez Sandin, M. Igarzabal, M. F. del Grosso, A. A. Valda, N. Canepa, M. Gun, D. M. Minsky, G. Conti, J. Erhardt, H. R. Somacal, A. A. Bertolo, J. Bergueiro, P. A. Gaviola, A. J. Kreiner, *Appl. Radiat. Isot.* **2020**, *166*, 109315.
[7] A. H. Soloway, W. Tjarks, B. A. Barnum, F.-G. Rong, R. F. Barth, I. M. Codogni, J. G. Wilson, *Chem. Rev.* **1998**, *98*, 1515–1562.
[8] P. Coghi, J. Li, N. S. Hosmane, Y. Zhu, *Med. Res. Rev.* **2023**, *43*, 1809–1830.
[9] A. Pitto-Barry, *Polym. Chem.* **2021**, *12*, 2035–2044.
[10] M. Lamba, A. Goswami, A. Bandyopadhyay, *Chem. Commun.* **2021**, *57*, 827–839.
[11] J.-D. Lee, M. Ueno, Y. Miyajima, H. Nakamura, *Org. Lett.* **2007**, *9*, 323–326.
[12] M. E. El-Zaria, H. Nakamura, *Inorg. Chem.* **2009**, *48*, 11896–11902.
[13] S. Kusaka, Y. Hattori, K. Uehara, T. Asano, S. Tanimori, M. Kirihata, *Appl. Radiat. Isot.* **2011**, *69*, 1768–1770.
[14] A. R. Genady, J. A. Ioppolo, M. M. Azaam, M. E. El-Zaria, *Eur. J. Med. Chem.* **2015**, *93*, 574–583.
[15] H. Koganei, S. Tachikawa, M. E. El-Zariaac, H. Nakamura, *New J. Chem.* **2015**, *39*, 6388–6394.
[16] A. Isono, M. Tsuji, Y. Sanada, A. Matsushita, S. Masunaga, T. Hirayama, H. Nagasawa, *ChemMedChem* **2019**, *14*, 823–832.
[17] I. Nakase, A. Aoki, Y. Sakai, S. Hirase, M. Ishimura, T. Takatani-Nakase, Y. Hattori, M. Kirihata, *ACS Omega* **2020**, *5*, 22731–22738.
[18] S. Hirase, A. Aoki, Y. Hattori, K. Morimoto, K. Noguchi, I. Fujii, T. Takatani-Nakase, S. Futaki, M. Kirihata, I. Nakase, *Mol. Pharmaceutics* **2022**, *19*, 1135–1145.
[19] A. Kim, M. Suzuki, Y. Matsumoto, N. Fukumitsu, Yukio Nagasaki, *Biomaterials* **2021**, *268*, 120551.
[20] T. Nomoto, Y. Inoue, Y. Yao, M. Suzuki, K. Kanamori, H. Takemoto, M. Matsui, K. Tomoda, N. Nishiyama, *Sci. Adv.* **2020**, *6*, eaaz1722.
[21] H. Nakamura, H. Koganei, T. Miyoshi, Y. Sakurai, K. Ono, M. Suzuki, *Bioorg. Med. Chem. Lett.* **2015**, *25*, 172–174.
[22] Y. Wang, G. Reina, H. G. Kang, X. Chen, Y. Zou, Y. Ishikawa, M. Suzuki, Naoki Komatsu, *Small* **2022**, *18*, 2204044.
[23] M. Nishikawa, H. G. Kang, Y. Zou, H. Takeuchi, N. Matsuno, M. Suzuki, N. Komatsu, *Bull. Chem. Soc. Jpn.* **2021**, *94*, 2302–2312.
[24] V. N. Mochalin, O. Shenderova, D. Ho, Y. Gogotsi, *Nat. Nanotechnol.* **2012**, *7*, 11–23.
[25] K. Turcheniuk, V. N. Mochalin, *Nanotechnology* **2017**, *28*, 252001.
[26] K. P. Loh, D. Ho, G. N. C. Chiu, D. T. Leong, G. Pastorin, E. K. H. Chow, *Adv. Mater.* **2018**, *30*, 1802368.
[27] M. D. Torelli, N. A. Nunn, O. A. Shenderova, *Small* **2019**, *15*, 1902151.
[28] P. Reineck, M. Capelli, D. W. M. Lau, J. Jeske, M. R. Field, T. Ohshima, A. D. Greentree, B. C. Gibson, *Nanoscale* **2017**, *9*, 497–502.
[29] T. D. Merson, S. Castelletto, I. Aharonovich, A. Turbic, T. J. Kilpatrick, A. M. Turnley, *Opt. Lett.* **2013**, *38*, 4170–4173.
[30] Y. Makino, T. Mahiko, M. Liu, A. Tsurui, T. Yoshikawa, S. Nagamachi, S. Tanaka, K. Hokamoto, M. Ashida, M. Fujiwara, N. Mizuoch, M. Nishikawa, *Diamond Relat. Mater.* **2021**, *112*, 108248.
[31] N. Komatsu, *Acc. Chem. Res.* **2023**, *56*, 106–116.
[32] M. Nishikawa, M. Liu, T. Yoshikawa, H. Takeuchi, N. Matsuno, N. Komatsu, *Carbon* **2023**, *205*, 463–474.
[33] Y. Zou, N. Komatsu, *Carbon* **2020**, *163*, 395–401.
[34] Y. Zou, S. Ito, F. Yoshino, Y. Suzuki, L. Zhao, N. Komatsu, *ACS Nano* **2020**, *14*, 7216–7226.
[35] Y. Zou, M. Nishikawa, H. G. Kang, G. Cheng, W. Wang, Y. Wang, N. Komatsu, *Mol. Pharmaceutics* **2021**, *18*, 2823–2832.
[36] S. Sotoma, R. Igarashi, J. Iimura, Y. Kumiya, H. Tochio, Y. Harada, M. Shirakawa, *Chem. Lett.* **2015**, *44*, 354–356.
[37] B. S. Miller, L. Bezinge, H. D. Gliddon, D. Huang, G. Dold, E. R. Gray, J. Heaney, P. J. Dobson, E. Nasatouli, J. J. L. Morton, R. A. McKendry, *Nature* **2020**, *587*, 588–593.
[38] L. P. Suarez-Kelly, S. H. Sun, C. Ren, I. V. Rampersaud, D. Albertson, M. C. Duggan, T. C. Noel, N. Courtney, N. J. Buteyn, C. Moritz, L. Yu, V. O. Yildiz, J. P. Butchar, S. Tridandapani, A. A. Rampersaud, W. E. Carson, *ACS Appl. Nano Mater.* **2021**, *4*, 3122–3139.
[39] D. Terada, S. Sotoma, Y. Harada, R. Igarashi, M. Shirakawa, *Bioconjugate Chem.* **2018**, *29*, 2786–2792.
[40] F.-J. Hsieh, S. Sotoma, H.-H. Lin, C.-Y. Cheng, T.-Y. Yu, C.-L. Hsieh, C.-H. Lin, H.-C. Chang, *ACS Appl. Mater. Interfaces* **2019**, *11*, 19774–19781.
[41] K. Kvakova, M. Ondra, J. Schimer, M. Petrik, Z. Novy, H. Raabova, M. Hajduch, P. Cigler, *Adv. Funct. Mater.* **2022**, *32*, 2109960.
[42] J. Barton, M. Gulka, J. Tarabek, Y. Mindarava, Z. Wang, J. Schimer, H. Raabova, J. Bednar, M. B. Plenio, F. Jelezko, M. Nesladek, P. Cigler, *ACS Nano* **2020**, *14*, 12938–12950.
[43] L. Zhao, A. Shiino, H. Qin, T. Kimura, N. Komatsu, *J. Nanosci. Nanotechnol.* **2015**, *15*, 1076–1082.
[44] L. Zhao, Y. H. Xu, H. Qin, S. Abe, T. Akasaka, T. Chano, F. Watari, T. Kimura, N. Komatsu, X. Chen, *Adv. Funct. Mater.* **2014**, *24*, 5348–5357.
[45] L. Zhao, Y. Nakae, H. Qin, T. Ito, T. Kimura, H. Kojima, L. Chan, N. Komatsu, *Beilstein J. Org. Chem.* **2014**, *10*, 707–713.
[46] H. Otsuka, E. Uchimura, H. Koshino, T. Okano, K. Kataoka, *J. Am. Chem. Soc.* **2003**, *125*, 3493–3502.
[47] T. Khan, K. Igarashi, A. Tanabe, T. Miyazawa, S. Fukushima, Y. Miura, Y. Matsumoto, T. Yamasoba, A. Matsumoto, H. Cabral, K. Kataoka, *ACS Appl. Bio Mater.* **2020**, *3*, 5030–5039.
[48] A. Doi, S. Kawabata, K. Iida, K. Yokoyama, Y. Kajimoto, T. Kuroiwa, T. Shirakawa, M. Kirihata, S. Kasaoka, K. Maruyama, H. Kumada, Y. Sakurai, S. Masunaga, K. Ono, S. Miyatake, *J. Neuro-Oncol.* **2008**, *87*, 287–294.
[49] T. Kageji, Y. Mizobuchi, S. Nagahiro, Y. Nakagawa, H. Kumada, *Appl. Radiat. Isot.* **2011**, *69*, 1823–1825.
[50] M. Nishikawa, H. Yagasaki, S. He, N. Komatsu, *ChemNanoMat* **2023**, *9*, e202300204.
[51] M. Sassi, L. Mascheroni, R. Ruffo, M. M. Salamone, G. A. Pagani, C. M. Mari, G. D'Orazio, B. La Ferla, L. Beverina, *Org. Lett.* **2013**, *15*, 3502–3505.
[52] J. Totobenazara, A. J. Burke, *Tetrahedron Lett.* **2015**, *56*, 2853–2859.
[53] P. Thirumurugan, D. Matosiuk, K. Jozwiak, *Chem. Rev.* **2013**, *113*, 4905–4979.
[54] H. Nulwala, K. Takizawa, A. Odukale, A. Khan, R. J. Thibault, B. R. Taft, B. H. Lipshutz, C. J. Hawker, *Macromolecules* **2009**, *42*, 6068–6074.
[55] P. Bendel, *NMR Biomed.* **2005**, *18*, 74–82.
[56] K. Kawai, K. Nishimura, S. Okada, S. Sato, M. Suzuki, T. Takata, H. Nakamura, *Mol. Pharmaceutics* **2020**, *17*, 3740–3747.
[57] L. Zhao, T. Chano, S. Morikawa, Y. Saito, A. Shiino, S. Shimizu, T. Maeda, T. Irie, S. Aonuma, H. Okabe, T. Kimura, T. Inubushi, N. Komatsu, *Adv. Funct. Mater.* **2012**, *22*, 5107–5117.
[58] Z. Guo, B. He, H. Jin, H. Zhang, W. Dai, L. Zhang, H. Zhang, X. Wang, J. Wang, X. Zhang, Q. Zhang, *Biomaterials* **2014**, *35*, 6106–6117.
[59] J. Hiratsuka, N. Kamitani, R. Tanaka, R. Tokiya, E. Yoden, Y. Sakurai, M. Suzuki, *J. Radiat. Res.* **2020**, *61*, 945–951.
[60] P.-P. P. Zhu Tang, M. P. Schweizer, K. M. Bradshaw, W. F. Bauer, *Biochem. Pharmacol.* **1995**, *49*, 625–632.
[61] Y. Zou, S. Ito, M. Fujiwara, N. Komatsu, *Adv. Funct. Mater.* **2022**, *32*, 2111077.
[62] L. Kou, J. Sun, Y. Zhai, Z. He, *Asian J. Pharm. Sci.* **2013**, *8*, 1–10.

Manuscript received: June 29, 2023
Accepted manuscript online: August 17, 2023
Version of record online: October 5, 2023

Minor changes have been made to Figure 2 since its publication in Early View.